

Nickel cobalt selenides on black phosphorene with fast electron transportation for high-energy density sodium-ion half/full batteries

Jun Yang^{a,b†}, Chenrui Zhang^{c,e†}, Jitao Geng^c, Yangyang Sui^c, Huaixin Wei^d,

Chencheng Sun^{a*}, Hongbo Geng^{c*}, Yushen Liu^{a*}

^aSchool of Electronic and Information Engineering, Changshu Institute of Technology,
Changshu, 215500, Jiangsu, China.

E-mail address: ccsun@cslg.edu.cn; ysliu@cslg.edu.cn

^bSchool of Material Science & Engineering, Jiangsu University of Science and
Technology, Zhenjiang, 212003, China

^cSchool of Materials Engineering, Jiangsu Key Laboratory of Advanced Functional
Materials, Changshu Institute of Technology, Changshu, Jiangsu 215500, China. E-
mail address: hbgeng@gdut.edu.cn

^dSchool of Chemistry and Life Sciences, Suzhou University of Science and
Technology, Suzhou, Jiangsu 215009, China

^eBTR New Material Group Co., Ltd., Shenzhen 518000, China

†These authors contributed equally.

Table of contents

- Fig S1.** XRD pattern of BP@Ni(OH)₂/Co(OH)₂ precursor.
- Fig S2.** XRD pattern of as prepared pure Ni₃Se₄/CoSe₂.
- Fig S3.** XPS survey spectrum of BP@Ni₃Se₄/CoSe₂.
- Fig S4.** XPS spectra of Se 3d in BP@Ni₃Se₄/CoSe₂.
- Fig S5.** Energy Dispersive Spectrometer (EDS) of BP@Ni₃Se₄/CoSe₂ and Ni₃Se₄/CoSe₂.
- Fig S6.** Nitrogen adsorption-desorption isotherm of BP@Ni₃Se₄/CoSe₂ and Ni₃Se₄/CoSe₂.
- Fig S7.** GCD curves of BP@Ni₃Se₄/CoSe₂ at different current densities.
- Fig S8.** Comparison of coulombic efficiency for the first 5 cycles.
- Fig S9.** Cycling performance of BP@Ni₃Se₄/CoSe₂ at 0.2 A g⁻¹.
- Fig S10.** Rate performance comparison of previously reported transition metal selenide-based electrode.
- Fig S11.** Rate and cycle stability of BP@Ni₃Se₄/CoSe₂ using NaClO₄ in EC/DMC as electrolyte.
- Fig S12.** Comparison of GITT curves of the cycled electrode.
- Fig S13.** Nyquist plots for the electrodes of BP@Ni₃Se₄/CoSe₂ and pure Ni₃Se₄/CoSe₂.
- Fig S14.** Morphology, crystal structure and performance in sodium ion batteries of NVPOF.

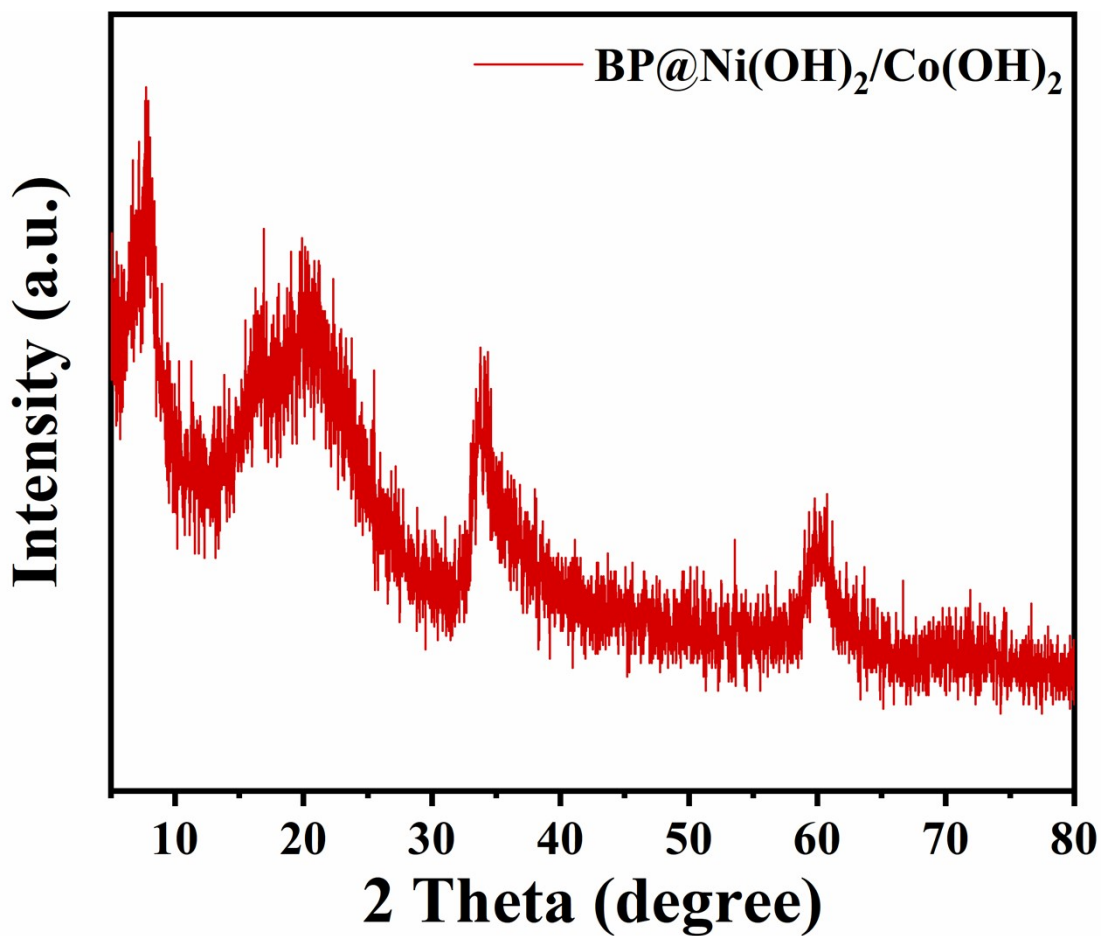


Fig S1. XRD pattern of BP@Ni(OH)₂/Co(OH)₂ precursor.

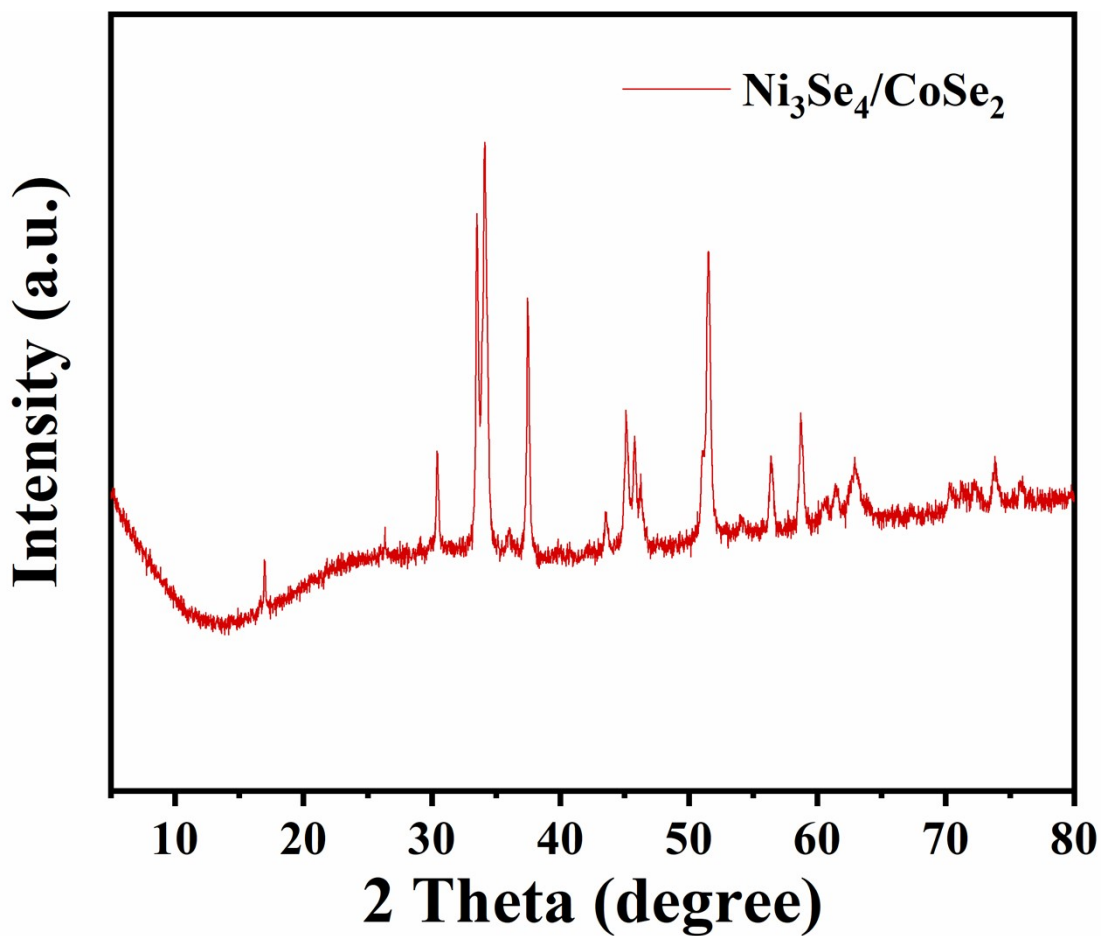


Fig S2. XRD pattern of as prepared pure $\text{Ni}_3\text{Se}_4/\text{CoSe}_2$.

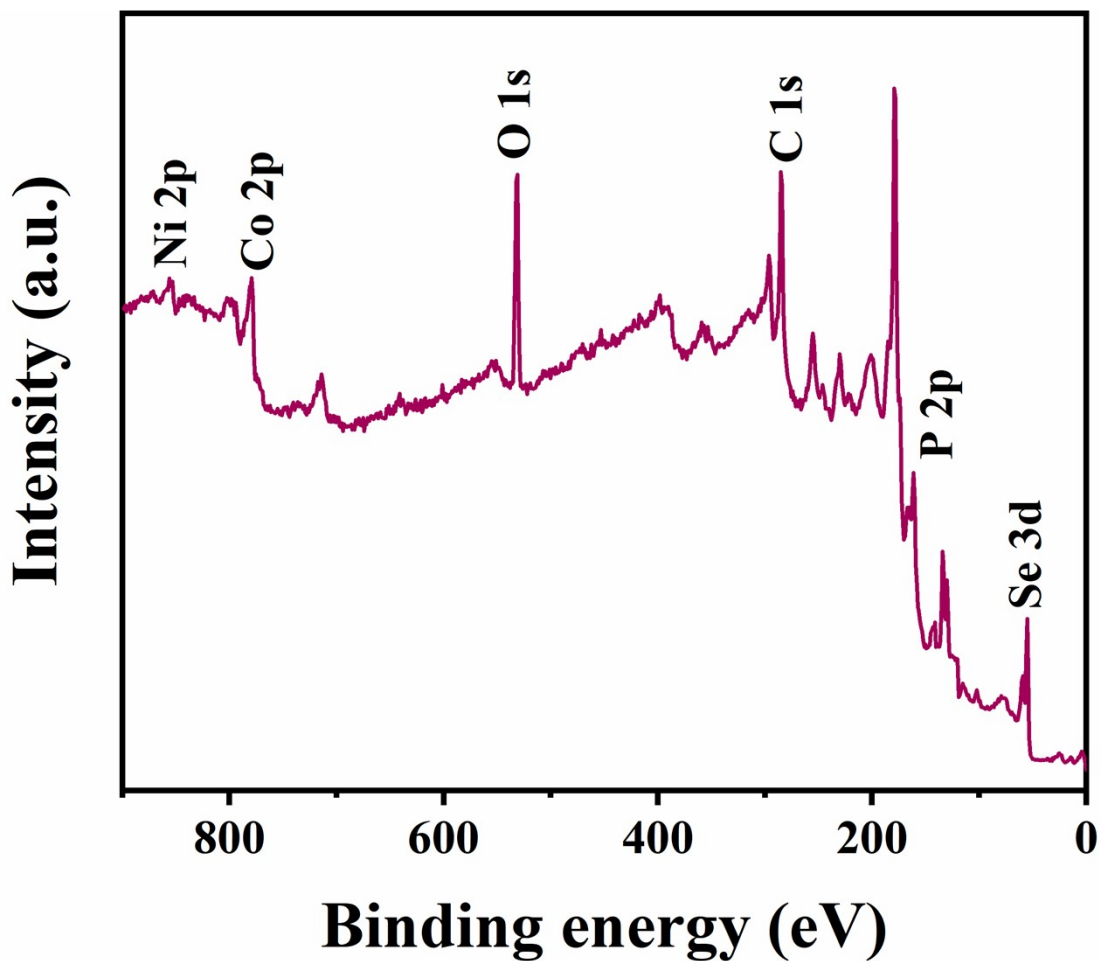


Fig S3. XPS survey spectrum of BP@Ni₃Se₄/CoSe₂.

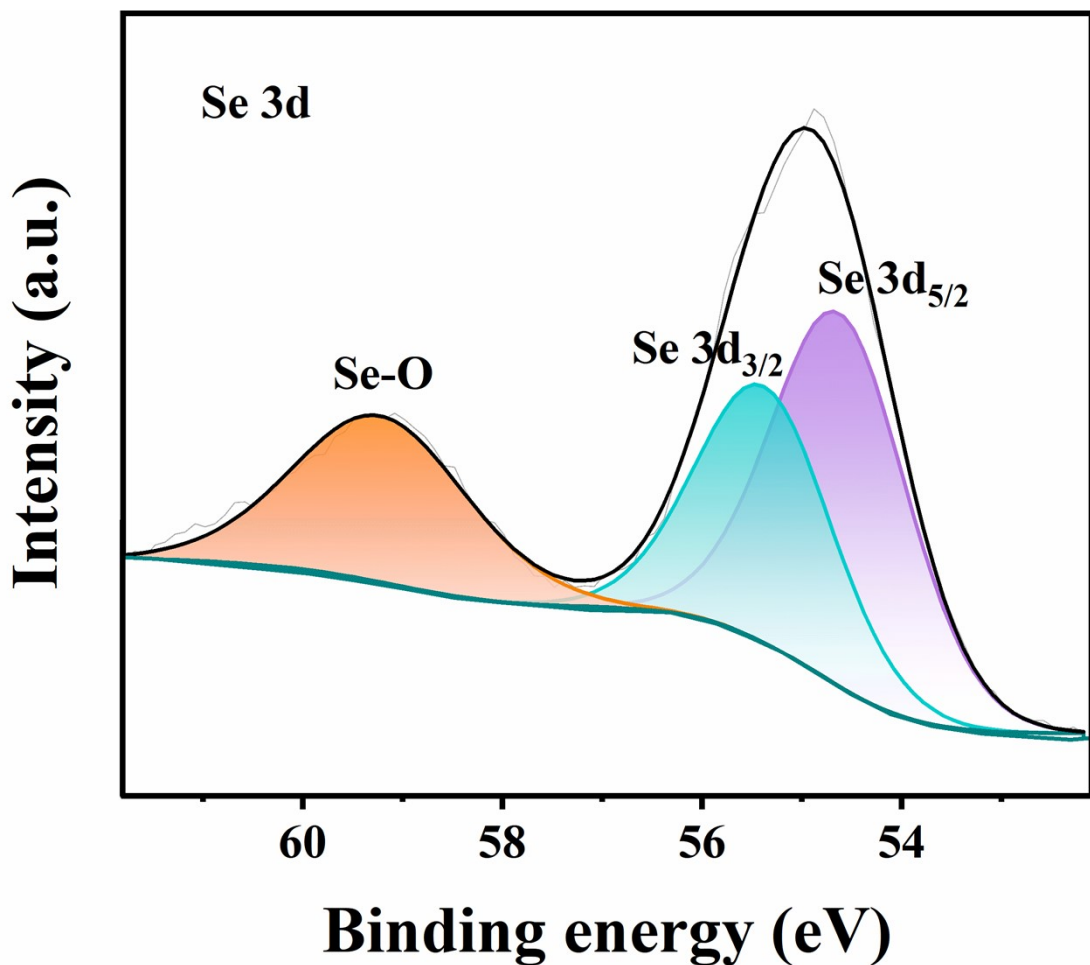


Fig S4. XPS spectra of Se 3d in BP@Ni₃Se₄/CoSe₂.

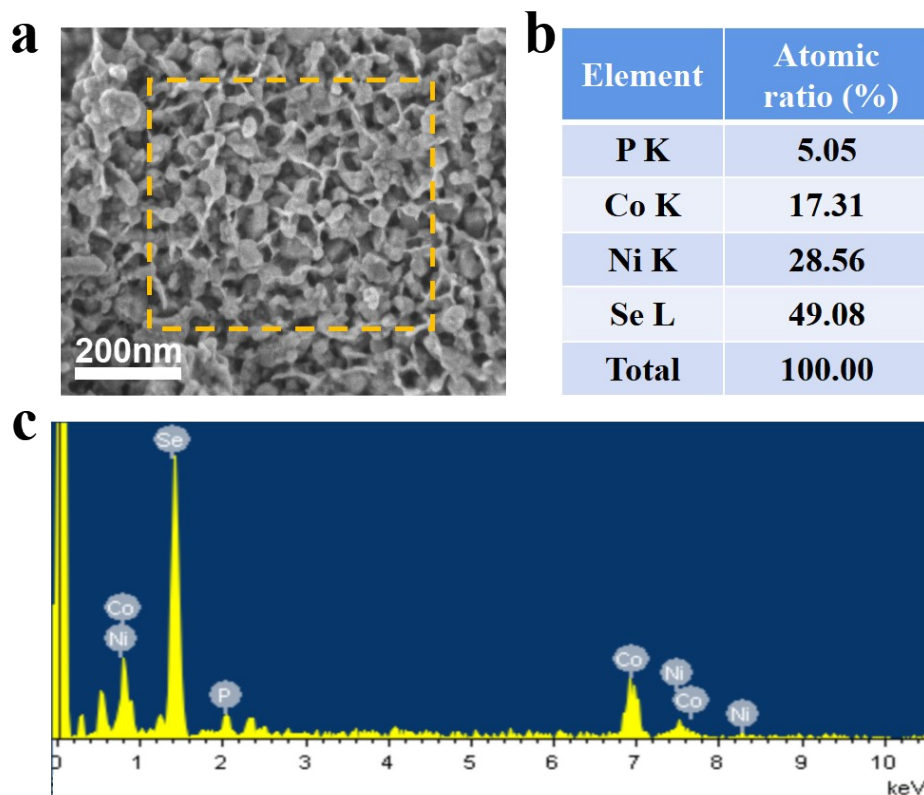


Fig S5. Energy dispersive spectrometer (EDS) of BP@Ni₃Se₄/CoSe₂. The mole ratio of BP, Ni₃Se₄ and CoSe₂ is about 17.1 %, 31.1 %, 51.8 % based on the atomic ratio.

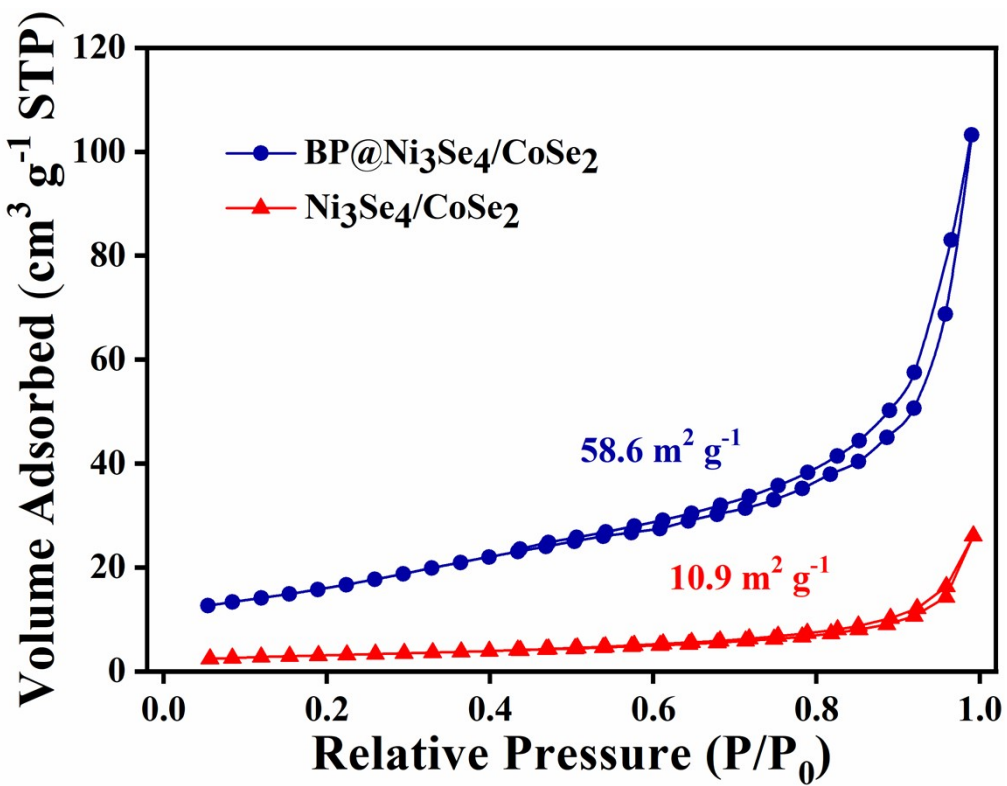


Fig S6. Nitrogen adsorption-desorption isotherms of BP@Ni₃Se₄/CoSe₂ and Ni₃Se₄/CoSe₂.

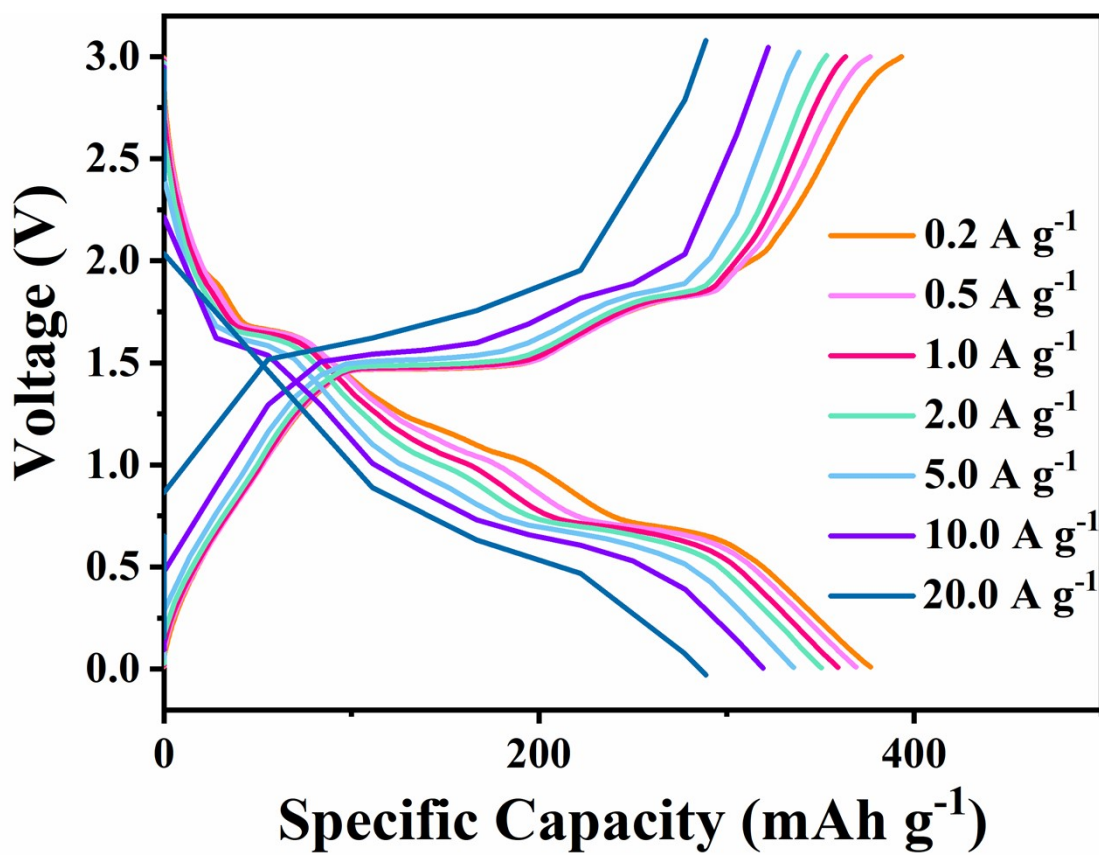


Fig S7. GCD curves of BP@Ni₃Se₄/CoSe₂ at different current densities.

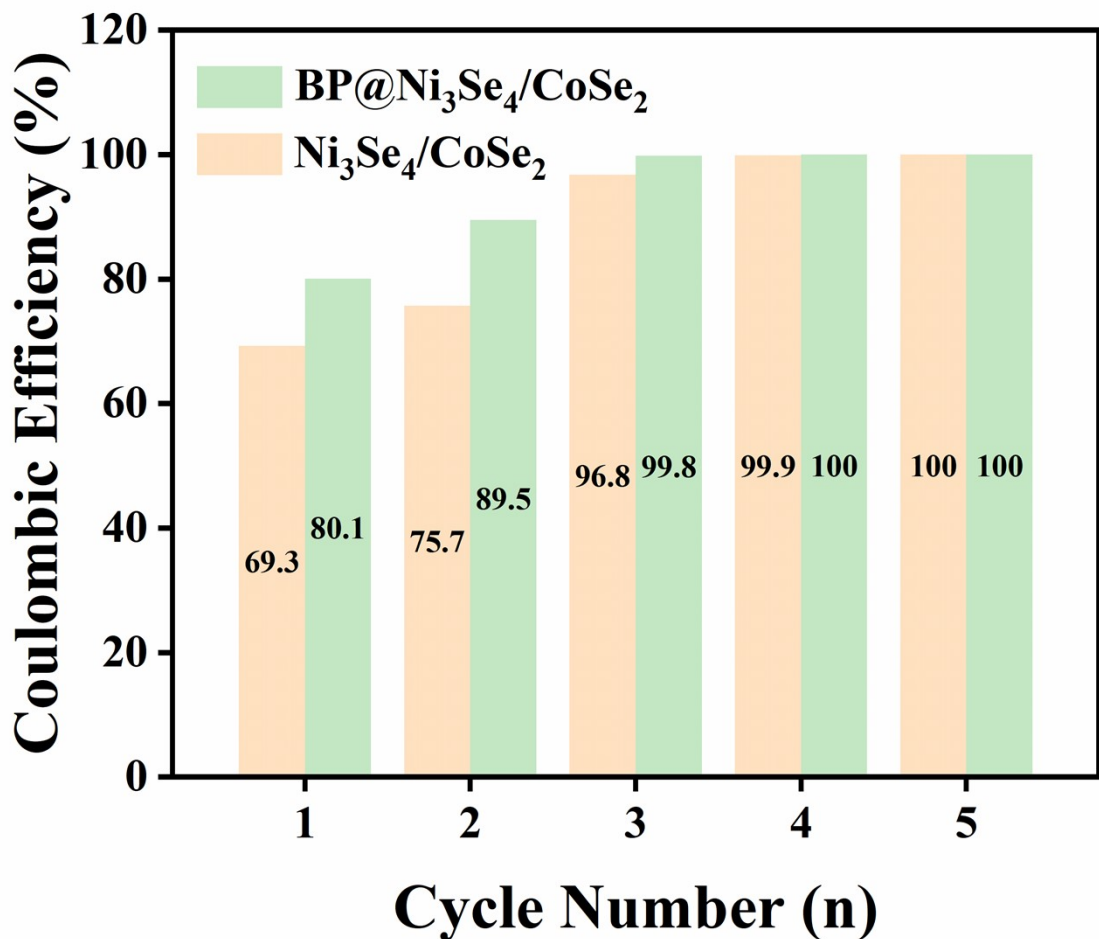


Fig S8. Comparison of coulombic efficiency for the first 5 cycles.

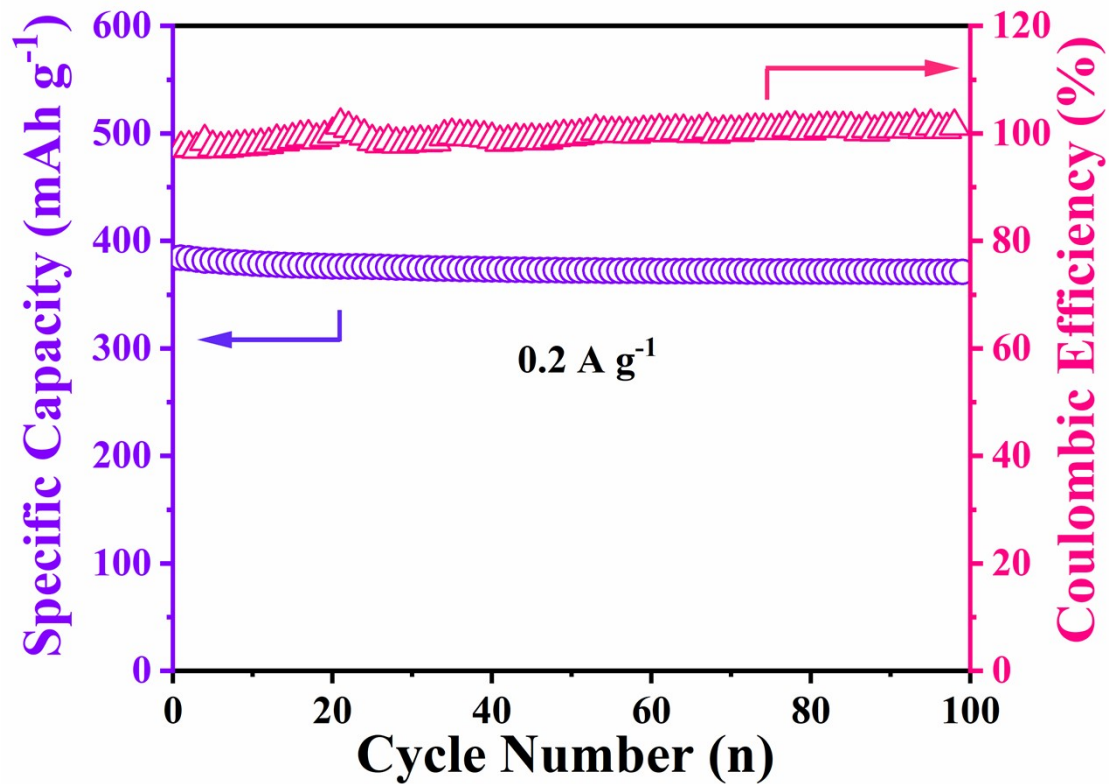


Fig S9. Cycling performance of BP@Ni₃Se₄/CoSe₂ at 0.2 A g⁻¹.

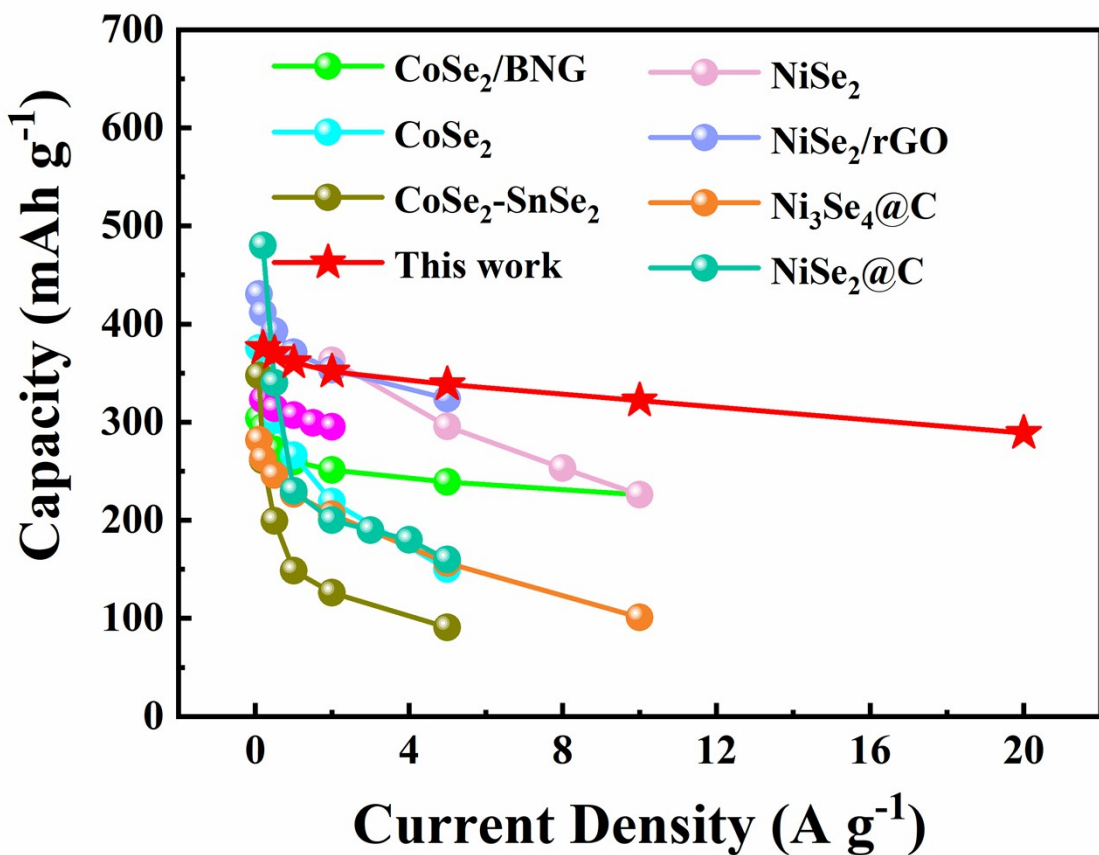


Fig S10. Rate performance comparison of previously reported transition metal selenide-based electrode.

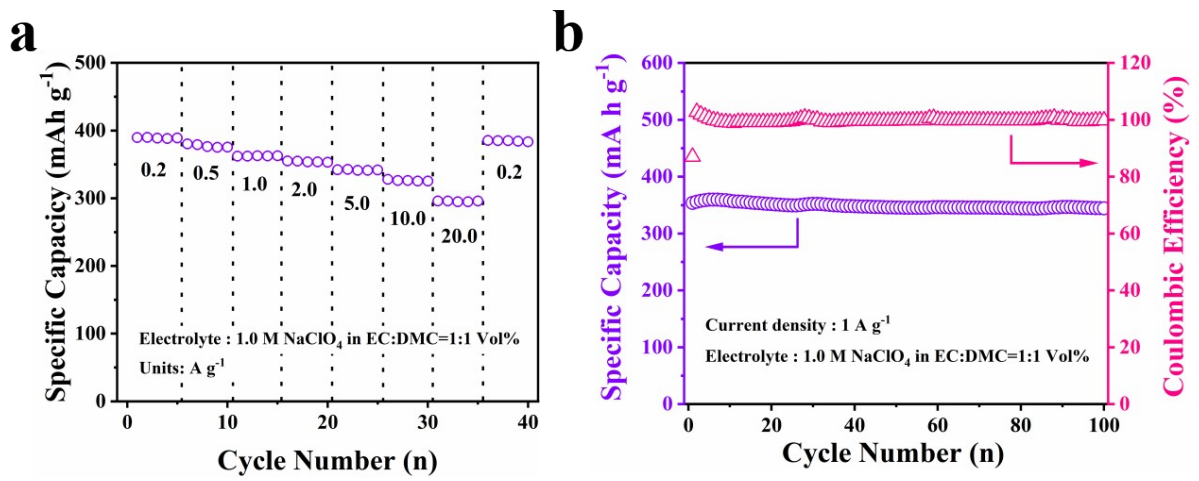


Fig S11. Rate and cycle stability of BP@ $\text{Ni}_3\text{Se}_4/\text{CoSe}_2$ using NaClO_4 in EC/DMC as electrolyte.

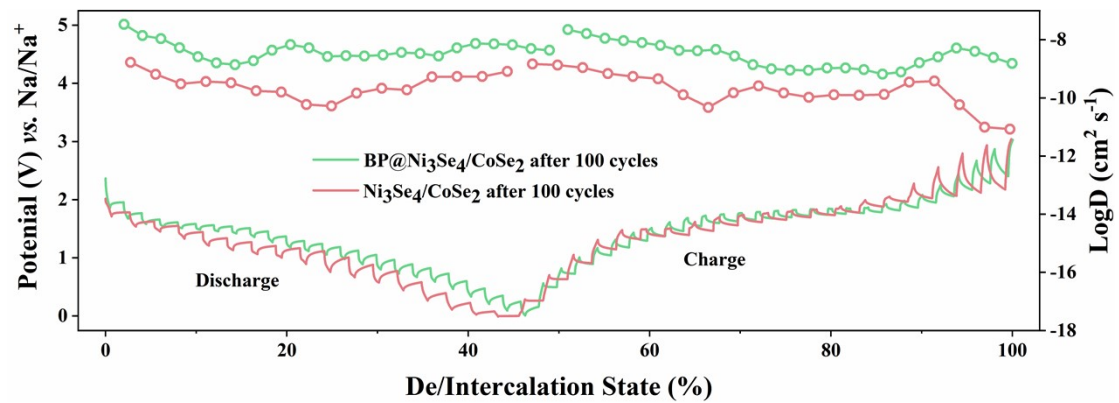


Fig S12. Comparison of GITT curves of the cycled electrode.

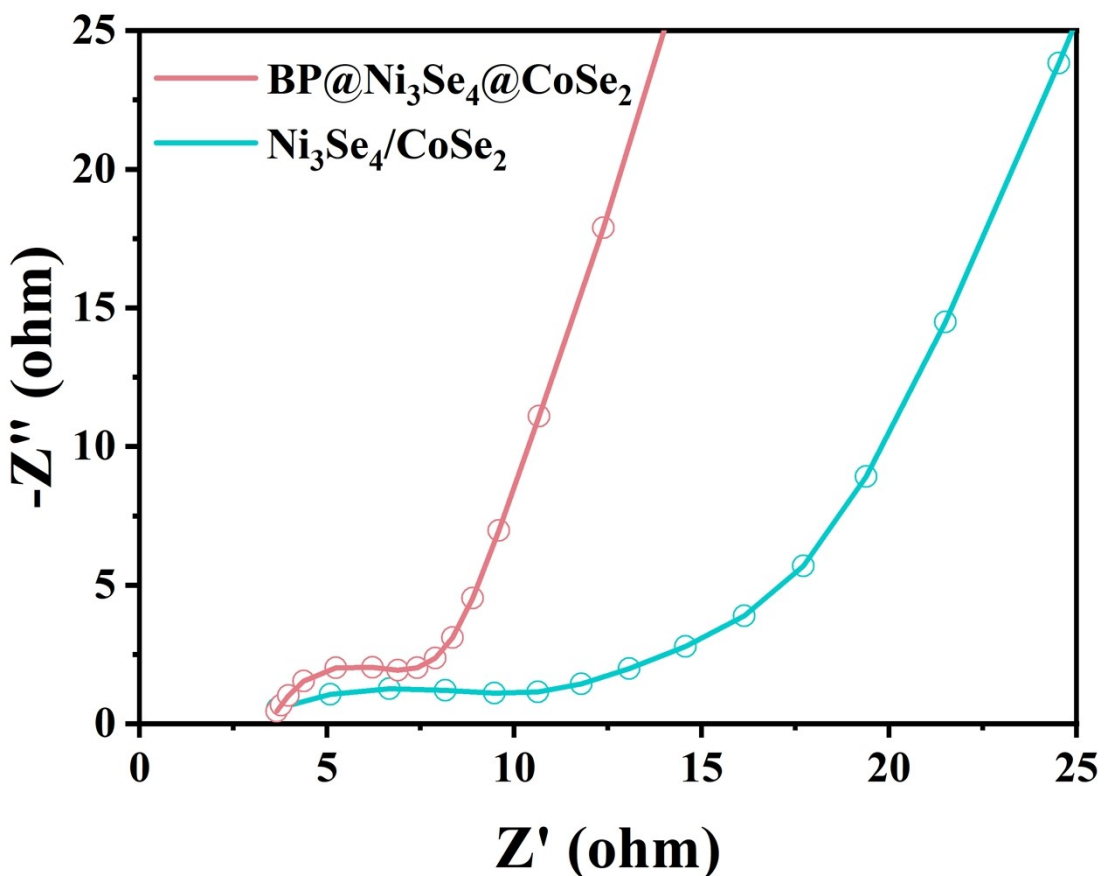


Fig S13. Nyquist plots for the electrodes of $\text{BP}@\text{Ni}_3\text{Se}_4/\text{CoSe}_2$ and pure $\text{Ni}_3\text{Se}_4/\text{CoSe}_2$.

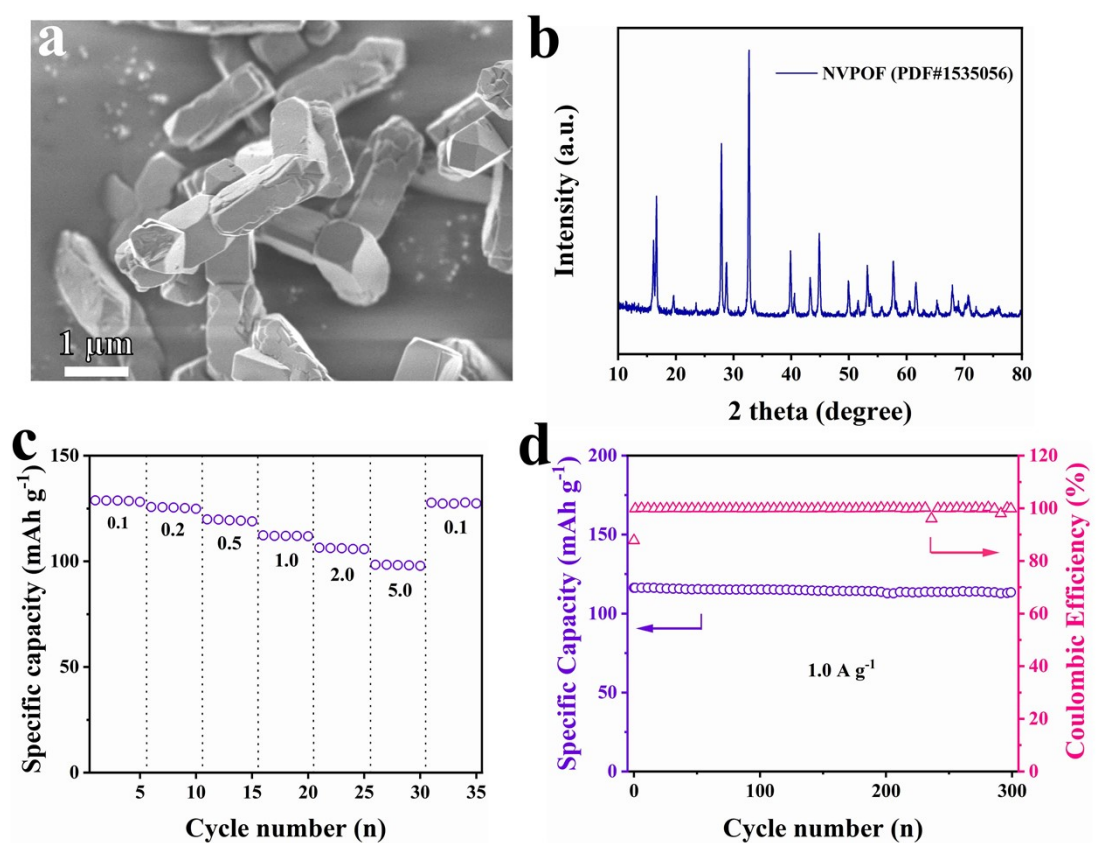


Fig S14. Characterization of NVPOF. (a) SEM image. (b) XRD pattern. (c) rate performance and (d) cycle stability.